Preferred citation: H. Eloranta, H. Lepomäki and T. Pärssinen. Fluid mechanics of the headbox nozzle: Coherent flow structures, instabilities and disturbances close to the nozzle exit. In **Advances in Paper Science and Technology**, *Trans. of the XIIIth Fund. Res. Symp. Cambridge, 2005*, (S.J. I'Anson, ed.), pp 51–81, FRC, Manchester, 2018. DOI: 10.15376/frc.2005.1.51.

FLUID MECHANICS OF THE HEADBOX NOZZLE: COHERENT FLOW STRUCTURES, INSTABILITIES AND DISTURBANCES CLOSE TO THE NOZZLE EXIT

Hannu Eloranta,[1] Hannu Lepomäki[2] and Tero Pärssinen[1]

[1]Institute of Energy and Process Engineering, Tampere University of Technology, P.O.Box 589, FIN-33101 Tampere, Finland
[2]Metso Paper Inc., P.O. Box 587, FIN-40101 Jyväskylä, Finland

ABSTRACT

In this study two sources of flow instabilities in the headbox nozzle are presented. Both of them appear close to the nozzle exit and therefore are easily conveyed to the slice jet. This makes their control critical in the view of the jet quality. These instabilities may lead to so-called "small scale faults" in sheet quality, which appear as cockle, fiber orientation streakiness and other small-scale dimensional stability problems. The first source of instability is the nozzle exit itself. The geometry of the nozzle exit is highly asymmetrical due to the slice bar in the upper lip. This results in sudden acceleration and streamline curvature. The results show that remarkable alterations in the structure of the turbulent boundary layer on the lower lip are observed due to the acceleration generated by a slice bar model. However, compared to the boundary layer turbulence, the flow structures evolving in the slice bar shear layer are an order of magnitude stronger. In essence, the slice bar model utilized in the present experiment creates strong streamwise vortices. The other instability is related to the tip of the vane. Recent experimental work has revealed the reason for stable MD-aligned streaks in the mean-flow field created by some vanes at certain speeds. The streaks results from a fluid-structure interaction, in which the flow excites the vane to respond in a characteristic vibration mode. This paper presents the effect of flow rate, vane tip thickness and vane material on this kind of streaking problem. Also the fundamental nature of the fluid-structure interaction, responsible for enhanced vortex shedding which is the mechanism the streaks are generated, is explained.

1 INTRODUCTION

The primary task of a papermaking machine headbox is to deliver pulp-suspension from the approaching system to the forming section by generating a plane free-surface jet. The headbox, together with the forming section, plays a major role in the production of high-quality paper and board, which typically means uniform sheet with desired properties. Sheet uniformity fundamentally means even basis weight and fiber orientation distributions. Commonly used quality measures include basis weight profiles, basis weight residual variation, formation, and fiber orientation profile. The absence of streakiness can also be considered as a quality measure reflecting the small-scale fiber orientation uniformity. An example of macro scale streakiness in paper sample is presented in Figure 1. In this Figure, a sheet of paper is set on a flat table and it is illuminated at a shallow angle. MD-aligned streaks are obvious in this sample. All solid particles like fibers, fines and fillers, as well as

Figure 1 MD-streakiness in a paper sample.

chemicals, should to be evenly distributed in the slice jet before the final freezing into the structure of paper takes place. To this end, the headbox has to generate and sustain certain level of turbulence to prevent flocculation of fibers and dispersion of the additives. In addition, a disturbance-free jet without secondary flows and other local non-uniformities is essential because any unevenness in the flow field may affect the quality of the final product. It has been shown that the properties of paper are strongly correlated with the headbox fluid mechanics; see e.g. references [1, 2, 3, 4, 5]. Both statistical and topological flow properties influence the paper structure. The term "headbox hydraulics" is used to refer to all these fluid mechanical phenomena that are relevant in producing a homogeneous slice jet and, therefore, good quality paper and board.

The design of the headbox hydraulics relies strongly on the appropriate distribution of fluidization energy, flow acceleration and control of turbulence properties [2]. The headbox hydraulics is typically optimized using computational fluid dynamics (CFD). Pilot scale trials also have an important role in the optimization. However, CFD models used typically in industrial applications are not able to predict all the aspects of the headbox flow. Especially, the occurrence of flow instabilities can only be studied experimentally, since models cannot include all the relevant parameters and their interactions. These flow instabilities may result in disturbances with considerable magnitude and thus inherit in paper. These phenomena have gained a lot more attention during the last few years since even higher quality requirements are set on paper and board products. Therefore, the traditional optimization of fluidization, profiles, turbulence properties and residence times are not the only requirements for high quality headbox hydraulics. Also effective control of flow instabilities developing separately from turbulence needs to be addressed.

In this study two sources of flow instabilities in the headbox nozzle are presented. Both of them appear close to the nozzle exit and therefore are easily conveyed to the slice jet. This makes their control critical in the view of the jet quality. These instabilities may lead to so-called "small scale faults" in sheet quality, which appear as cockle, fiber orientation streakiness and other small-scale dimensional stability problems, as discussed in the reference [1].

The first one is the nozzle exit itself. The sudden change of boundary conditions from accelerating channel flow to a free-jet has a strong influence on the flow. This point has also been studied in [6]. In addition, the geometry of the nozzle exit is highly asymmetrical due to the slice bar in the upper lip. Resulting sudden acceleration and streamline curvature are sources various fluid mechanical phenomena, which will be examined and discussed here. This survey stems from the fact that in many cases paper sheet shows considerable variation of quality and characteristics between the surfaces. One possible source of this variation might be the highly asymmetrical configuration of the headbox nozzle exit. Flow around the slice bar and related instabilities have previously been studied in [7]. That work has later been extended in [8] and [9] to cover the entire nozzle exit, i.e. also the bottom lip boundary layer. The latter two studies with some additional considerations from the paper making point of view will be revisited here. The objective is to show and explain the nature of instabilities generated by the slice bar and study the effect of slice bar to the overall flow dynamics of the nozzle exit.

The second source of instability is the tip of the vane. Vanes of different length are commonly used in headboxes. Typically the vanes end inside the nozzle somewhat upstream of the slice bar, but in some applications they may also extend to the jet. The primary flow instability related to the vane tip is the Strouhal instability, which results in the generation of coherent spanwise vorticity. The inheritance of this instability to paper has been studied in [3]. This study showed that the scale of vortices shedding from the vane tip inherits in paper structure. Furthermore, this scale is directly related to the actual thickness of the vane tip. However, a more complicated flow pattern has been observed in the wake of the vane, which will be shown to result from a fluid-structure interaction (FSI). Under certain circumstances, FSI induced the vane to vibrate and in this way creates a CD-periodic secondary mean-flow pattern, which characteristics has also been detected in paper samples. The objective of this part is to study the details of vortex shedding, determine the vibration mode of the vane, and show their coupling in terms of fluid-structure interaction.

2 EXPERIMENTS

All the experiments described in this paper are performed with in pure water without pulp-fibers suspended. This approach needed to be chosen, since the experimental techniques utilized to study the flow properties and structural vibrations require clear optical access to the measurement point. Wood fibers as an opaque material prevent the usage of measurement techniques based on optical imaging, such as PIV. Presently, such a powerful tool as PIV to measure the flow topology and spatial organization, does not exist for opaque pulp-suspension flows. Fortunately this is not a substantial deficiency, since the instabilities of interest are fluid mechanical in nature and the fibers do not play an important role in the generation of such instabilities. Naturally, the presence of the second phase, i.e. fibers, does affect the development of these instabilities and consequently to the overall fluid dynamics. The major impact of fibers to the fluid dynamics is seen to dampen turbulent and other velocity fluctuations and increase dissipation [10]. Therefore, measurements in pure water are expected to show the same fundamental dynamics as pulp-suspension, but the relative importance of various mechanisms and energy containing scales may differ from those present in real processes. The fundamental similarity between pure water and pulp-suspension flow is evident also by comparing previous studied linking the laboratory-scale water experiments with measurements in a pilot-scale paper machine [3].

2.1 Measurement equipment

A short description of the measurement equipment is provided here. All techniques utilized in the next sections are well established and a vast amount of literature can be found on the applicability and accuracy of each technique. The following text only summarizes the principles, the type of data obtained with each technique and some references to find more information.

Flow Visualization (FV)

FV was probably the first technique used to study fluid flows. This technique is not limited to any particular set of hardware. A typical setup includes a light source, some dye, smoke or tracer particles injected to the flow and a camera to record images of the illuminated dye etc. The results in Figure 11, are obtained by injecting fluorescent dye through a narrow slot in the nozzle top wall and illuminating the flow with a laser-sheet. Dye passing the laser sheet emits light, which is recorded by a CCD-camera. Vortices and other flow structures concentrate and diffuse the dye, so that their imprint can be seen in the distribution of dye.

Particle Image Velocimetry (PIV)

PIV is a technique to measure instantaneous flow velocities over a 2D-domain. In contrast to other conventional flow velocity measurement techniques, PIV is able to capture an instantaneous snapshot of the entire flow field at once. Hotwire Anemometry (HWA) and Laser Doppler Anemometry (LDA) are only able to sample velocity data in one measurement point at time. Therefore PIV enables to study topology and coherent structures in the flow in a very powerful way. Extensions to standard PIV technique, such as High-speed PIV and Stereoscopic-PIV make it possible to sample instantly all three components of velocity over a spatial 2D domain at several kHz sampling rate. PIV is based on optical imaging of small tracer particles seeded to the flow. The particles are illuminated by a laser sheet and imaged by a CCD-camera. A special algorithm is used to compute the displacement of particles from frame to frame and this information is transformed into velocity as the time difference between the frames is known. Details of this technique can be found in [11] and references therein.

Laser Vibrometer (LV)

LV is used to measure vibration of solid surfaces. Its idea is actually very close to that of LDA for fluid velocity measurement. In this technique, a laser beam is focused to a surface and the reflecting diffraction pattern is detected and analyzed to compute the velocity of the surface. The measurement can be performed at several kHz sampling rate. So, in essence, one obtains a velocity signal from the surface, from which the vibration spectrum can be estimated. In normal systems only the component of velocity parallel to the laser beam can be measured. However, techniques have been developed to measure also the other components and the rotation of the surface. If several points on the surface are measured, this data can be used for modal analysis, which yields the mode of vibration related to a specific frequency of vibration. A thorough explanation of this subject can be found in the reference [12].

2.2 Apparatus

In section 3, the flow through the exit of the headbox nozzle and around the slice bar is studied. This is done by reproducing the fundamental fluid dynamics in a very simplified geometry. The design of the last section of the headbox nozzle, which is actually forming the jet, is illustrated in Figure 2a.

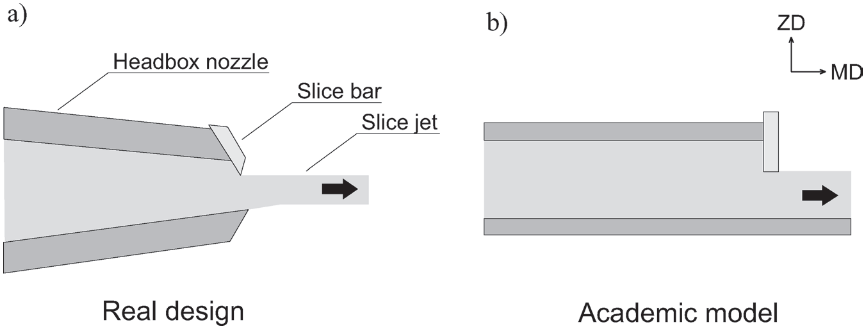

Figure 2 Slice bar in the headbox nozzle (a), the design of the simplified nozzle and slice bar model used in the experiments (b).

Figure 2b shows the simplified design used in these experiments. From the fluid mechanical point of view, the geometry of interest is essentially a 2D-contraction with one-sided blockage at the nozzle exit. In this study, the contraction of the nozzle is neglected and the nozzle is modeled as a plane channel. The construction of the slice bar is also simplified. In the model a right-angled 2:1 blockage is mounted to the upper wall. This high blockage ratio is used to intensify the instabilities to be studied. Thus, one should be careful in making too straightforward conclusion about the effect of the slice bar in real processes. In the present setup, the development of the jet downstream of the slice bar cannot be studied. Experiments are performed only inside the nozzle to understand the role of flow instabilities and large-scale flow structures to the jet quality. Further details of the setup and the water tunnel where the model is installed, are provided in references [7, 8, 9].

Experiments on the effect of vanes are carried out in a more realistic setup. The vane is placed in a laboratory-scale headbox nozzle test rig. A schematic drawing of the test rig is provided in Figure 3. The vane is hinged to the end of a turbulence generator tube bank, which is a replica of that used in real machines. Also the contraction angle of the nozzle is close to that typically used in the production machines. The vane is made of polycarbonate with the last 60mm tapered from the body thickness of 3mm to 1mm at the tip. This thick tip is used, since all the phenomena are much more evident with a thick trailing edge. Experiments have shown that the nature of vortex shedding

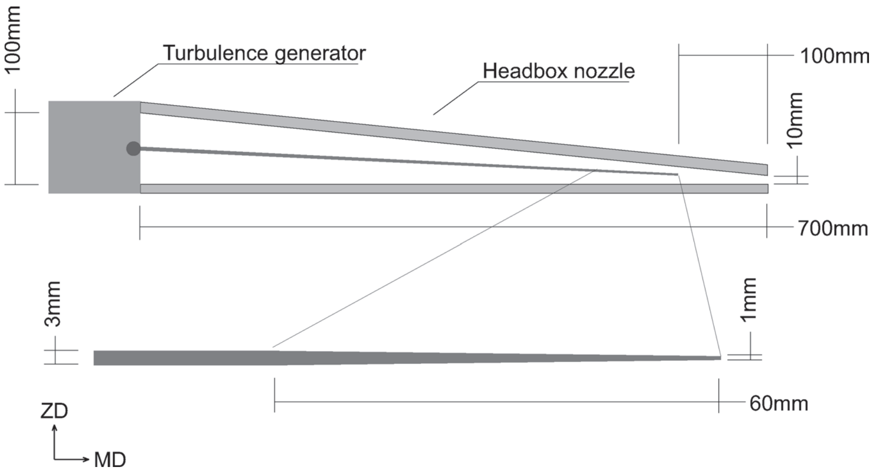

Figure 3 Design of the headbox nozzle test rig and dimensions of the vane used in the experiments.

does not change as the tip thickness is varied between 2mm and 0.25mm. Only the scale and magnitude of the phenomena change. The thickness of a typical production vane tip is about 0.5mm. In this case, the vane ends 100mm before the nozzle exit. Further dimensions of the test rig are not provided here, since they are not relevant to the vortex shedding at the vane tip and resulting fluid-structure interaction (FSI). It must be pointed out, that similar FSI response has been reproduced in an academic model, with laminar inlet profile and the vane clamped to the end of a wing-profile with elliptical leading edge. To put another way, the FSI described in section 4 is rather insensitive to the upstream conditions and only the type of the vane is important. Figure 4 shows the measurement planes and their location in respect to the vane tip. Solid and dashed lines denote PIV measurement planes (for the fluid velocity) and dotted lines the LV measurement area (for the vane vibration). PIV experiments are typically conducted both in the MD-CD- and MD-ZD-planes. The former is the plane, in which the secondary flows (streaks) appear most clearly and the latter is normally used to look at the characteristics of vortex shedding. Details of the measurement technique and data processing algorithms are provided in references [13, 14].

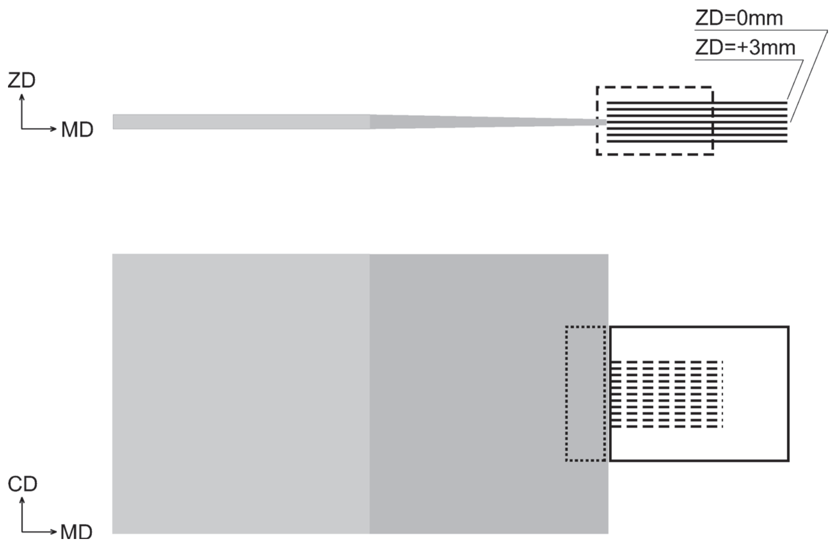

Figure 4 Locations and labeling of the measurement positions in the wake of the vane. Solid line corresponds to the PIV-measurements in the MD-CD –plane, dashed in the MD-ZD –plane and dotted to the area of LV measurement domain on the vane surface.

3 FLOW AROUND THE SLICE BAR

In this section results from the academic nozzle and slice bar model explained in section 2.2 are presented. Prior to the experimental results, some background on the physics related to the present configuration is outlined.

3.1 The effects of sudden acceleration and streamline curvature

As described above, the headbox nozzle equipped with a slice bar can be modeled as a plain channel with one-sided forward-facing step (FFS) at the channel exit. The FFS generates an intense streamwise acceleration and streamline curvature as the flow passes by the blockage. In this study particular attention is paid to the evolution of the bottom wall boundary layer, since it is known to be populated by coherent flow structures [15]. Therefore, considering the small-scale disturbances, the layers close to the bottom lip and the slice bar are far more interesting than the bulk flow.

The effects of acceleration to a turbulent boundary layer have been studied extensively in the literature [16, 17, 18, 19, 20, 21]. Experiments both with constant streamwise pressure gradient and spatially varying acceleration have been performed. The main conclusion from the literature is that a strong enough acceleration can revert initially turbulent boundary layer into a quasi-laminar state, which resembles a laminar boundary layer. The change takes place gradually in a process where relative turbulence intensity decreases especially in the mid-boundary layer and low-frequency patches appear to the flow. During the relaminarization energy shifts to the larger scales. The boundary layer streaks become highly elongated in the streamwise direction. Eddies decrease in number and are more oriented in the streamwise direction. From the headbox point of view the effects of streamwise acceleration have been studied in [22]. Usually the magnitude of acceleration is quantified by a non-dimensional acceleration parameter K, which is defined as:

$$K = \frac{\nu}{U_E^2} \frac{dU_E}{dx} \tag{1}$$

, where ν is the kinematic viscosity (m^2/s) and U_E is the free-stream velocity (m/s). Even though it is obvious that this parameter cannot solely characterize the development of a boundary layer under acceleration, it seems that the value of $K > 3.0\times10^{-6}$ is a critical requirement for the relaminarisation to take place. Despite the numerous studies, unambiguous definition or parameter to mark the onset of relaminarisation has not been established. This is predominantly due to the gradual changes and somewhat overlapping boundaries between different phases in the laminarisation. In the typical headbox applications, the value of K is well below the critical level, but the acceleration due to the slice bar model increases the level of K over the critical level for a short period. Total relaminarization of the flow is not easily achieved even if the level of K exceeds the critical value, since also the duration of intense acceleration is important. However, the trend of decaying turbulence obvious in slice chamber.

In contrast, there are not so many publications on the effect of FFS or other similar blockages in the channel flow. The effect of streamline curvature has gained some attention in the literature. Previous work on the fluid dynamics of the slice bar has also been focused on the instabilities generated by the streamline curvature [7]. This work showed that besides creating an intense acceleration, the slicebar is a remarkable source of instability. In the time-mean frame, a spanwise vortex is developed in the corner of the top-wall and the slice bar model. Examination of instantaneous velocity fields reveals that this vortex is neither fixed in location nor constant in size. Occasionally more than one spanwise vortex appears in the corner. Instantaneous velocity fields measured in the CD-ZD-plane show that also streamwise vortices are generated upstream of the FFS. These vortices first appear in the upstream close to the top-wall. To the down-stream direction they move away from the top-wall and pass under the edge of the FFS. The origin of these streamwise vortices appears to be strong shear and embedded instability mechanisms.

3.2 Results on the effect of the slice bar

First a short description of the statistics measured on the bottom wall is presented. This is done to characterize the state of the boundary layer and its' development under acceleration due to the slice bar model. Figure 5 illustrates the time-mean flow pattern close to the FFS by means of the streamlines. The flow is from left to right. The vortex developing in the corner of the slice bar model and the top wall is evident in this image. Also the decrease of the bottom wall boundary layer thickness is clearly observed as the streamlines are collapsing closer to the bottom wall under the FFS. This figure also presents the coordinate system. MD is denoted by x, but positive x runs to the upstream direction, so that x-coordinate indicates the distance from the slice bar. ZD is denoted by y and CD by z. The origin of the coordinate system is located just under the FFS indicated by a black dot. Also the location of the CD-ZD measurement planes is presented in Figure 5.

The streamwise evolution of the acceleration parameter K is presented in Figure 6. The maximum of K achieved at around x=20mm is 6.75×10^{-6}. After

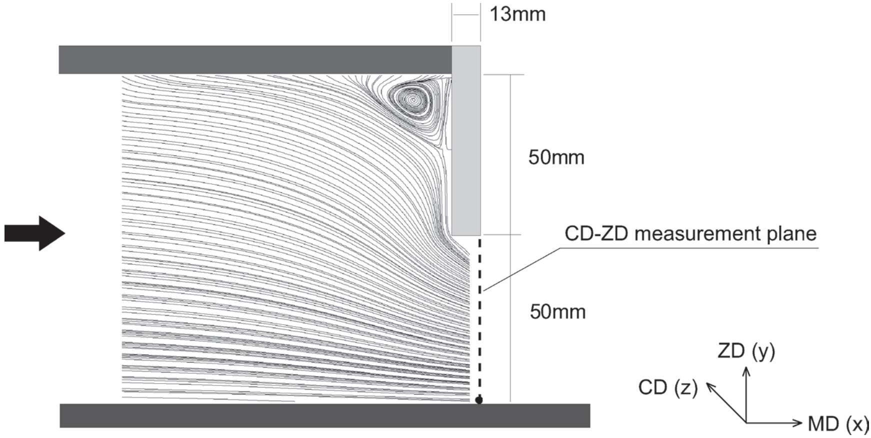

Figure 5 Mean flow pattern in terms of streamlines at the exit of the model. The flow direction is indicated by the arrow. The location of the measurement position just under the FFS in the CD-ZD-plane is indicated in the figure. Also the coordinate system and the origin (the dot under the FFS) are shown.

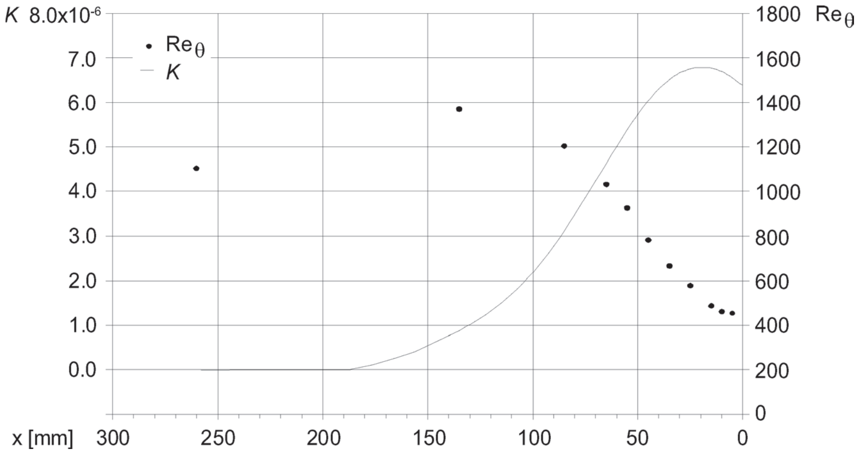

Figure 6 Streamwise development of the acceleration parameter K and the Reynolds number based on the boundary layer momentum thickness Re_θ.

this peak, the acceleration parameter starts to decrease. Figure 6 also shows the development of the Reynolds number based on the boundary layer momentum thickness, Re_θ. Reynolds number diminishes at a constant rate between *x*=85mm and *x*=20mm, after which the drop slows down. Re_θ remains at around 450 as the flow exits the channel. The mean-velocity profiles at the downstream positions are strongly distorted by the presence of the FFS. The maximum velocity is located on the edge of the boundary layer, which suggests that the influence of the FFS penetrates close to the opposite wall. Plotted with the real distance from the wall on the *y*-axis, these profiles show that the boundary layer thickness decreases towards the slicebar (not shown here). The development of turbulence is depicted by plotting streamwise profiles for $U_{x,rms}$ and $U_{y,rms}$. This is done by choosing three streamlines, along which the intensities are followed. Streamlines are identified by a constant value of a stream function, which is defined as:

$$\frac{\psi}{\nu} = \frac{1}{\nu} \int_0^y U(y)\, dy \tag{2}$$

where ν is the kinematic viscosity (m^2/s), U the velocity (m/s) and y the distance from the wall (m). The streamline at ψ=15000 is on the edge of the boundary layer. Development in the mid-layer is examined at the level ψ=3000. Even though the resolution close to the wall is only moderate, ψ=1000 is chosen to represent the near-wall area. In Figure 7, the velocity

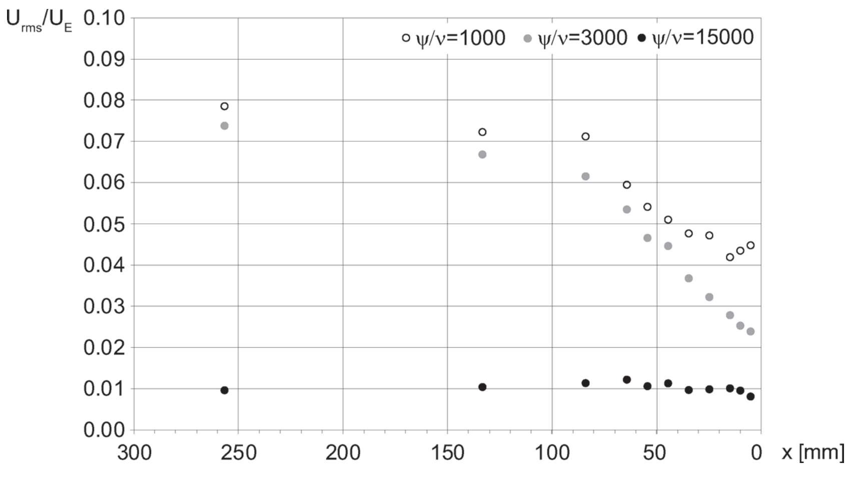

Figure 7 Streamwise profiles of the turbulence intensity for U_{MD} along three streamlines.

rms-values are normalized by U_E, i.e. the local free-stream velocity. Outside the boundary layer the turbulence intensity remains essentially constant, but in the mid-boundary layer the turbulence intensity decreases significantly. The peak of $U_{x,rms}$ close to the wall cannot be accurately resolved due to the extremely small boundary layer thickness. Over most of the positions, the trend of decaying turbulence intensity is obvious at least down to ψ=1000. However, close to the position x=0mm the decrease is slowed down or even halted. Actually, over the last few downstream positions, the level of $U_{x,rms}$ is increasing in absolute terms, i.e. without scaling by U_E.

Next, two instantaneous flow fields in the *y*-*z*–plane are presented. Both fields are measured just under the downstream edge of the FFS. The uppermost row (large frames) in Figure 8 cover the entire channel height under the step, as presented in Figure 5. The small frames below are cropped from the bottom of the first one and re-scaled. This is done to visualize the boundary layer structures, which are almost an order of magnitude weaker than those present in the FFS shear layer. The contours in the background represent streamwise vorticity ω_{MD} and the vectors the velocity fluctuations in this plane according to the Reynolds decomposition. In the large images, the scale of vorticity is set to ±500 1/s and in the small ones to ±100 1/s. The first example (left column) shows one very strong vortex pair beneath the edge of

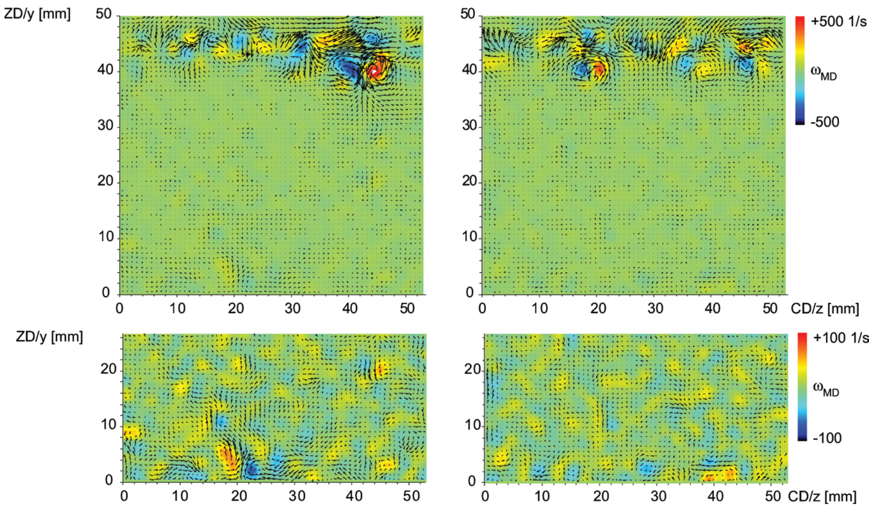

Figure 8 Two examples of instantaneous flow fields in the CD-ZD-plane just under the FFS. Small frames represent the lower part of the original field re-scaled to better adduce the boundary layer structures.

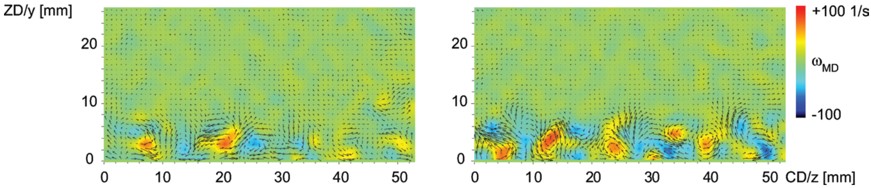

Figure 9 Two examples of instantaneous flow fields in the CD-ZD-plane measured in the upstream turbulent boundary layer.

the FFS and a rather weak vortex pair in the bottom wall boundary layer. On the bottom wall, the flow field appears to be quite smooth, which is interpreted as a consequence of relaminarisation. The second example portrays a few smaller scale vortex pairs in the step-shear layer. The small frames can be compared with Figure 9, which shows two instantaneous fields measured in the upstream at x=250mm. This location is in the region, where acceleration is not acting yet and the boundary layer can be considered as fully turbulent. Again the contours in the background represent streamwise vorticity and the scale is ±100 1/s. In both frames streamwise vortices fill the whole span across the window. They are also stronger than in the downstream position. It can be stated (based on the examination of hundreds of frames) that the number of streamwise vortices in the boundary layer decreases significantly under acceleration. This observation is in accordance with the results in Figure 7 showing reduced turbulence activity in the downstream positions. To address the questions of the vortex generation and their time-scales in the FFS shear layer, PIV-data is used to produce time-sequences of vorticity. This is performed by extracting one row of data in each velocity field and combining consecutive rows into a new plot with CD-location on the x-axis and time on the y-axis. The camera frequency is only 10Hz, but since strong vortices remain at fixed positions over the period of several frames, estimation of the scale of the largest vortices can be deduced. Figure 10 presents three this kind of vorticity time-sequences. Time resolution is 0.1s and by using the mean convective velocity of 2.0m/s this corresponds to a spatial resolution of 0.2m. Even though it is not clear if vorticity that remains at a fixed location over several frames indicates a single vortex pair or a sequence of individual vortex pairs, which are triggered and born one after another, the vorticity forms extremely large-scale structures. In the figures the spanwise wandering of the vortices seems to be remarkable, but it has to be emphasized that it is only in the order of 20mm. On the other hand, the time-scale of the structures may be as large as 10 frames (1 second), which corresponds to 2m in length.

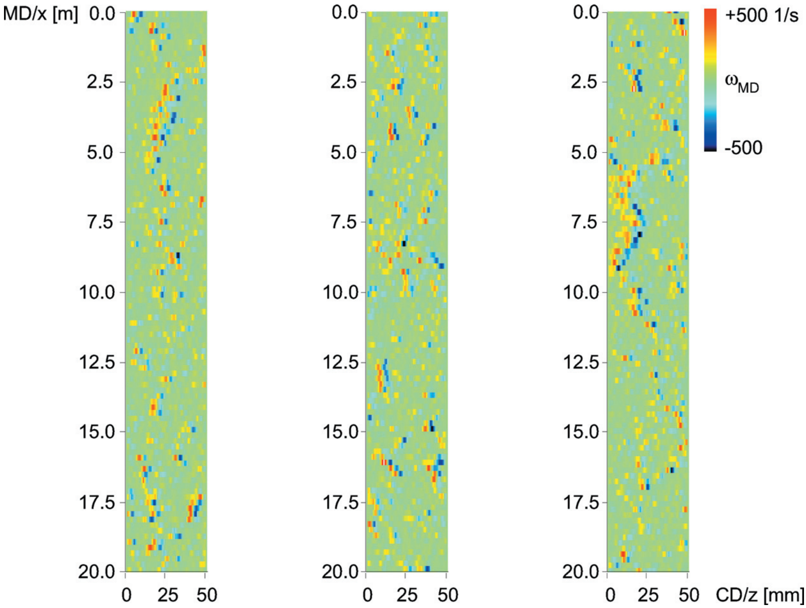

Figure 10 Three vorticity time-sequences in the step shear layer.

Similar analysis in the boundary layer does not indicate any large-scale vortices.

Figure 11 presents two frames from the flow visualizations performed in the y-z – plane just under the step. The same phenomena as in the Figure 8 can be observed here. Large-scale vortex pairs in the step shear layer are

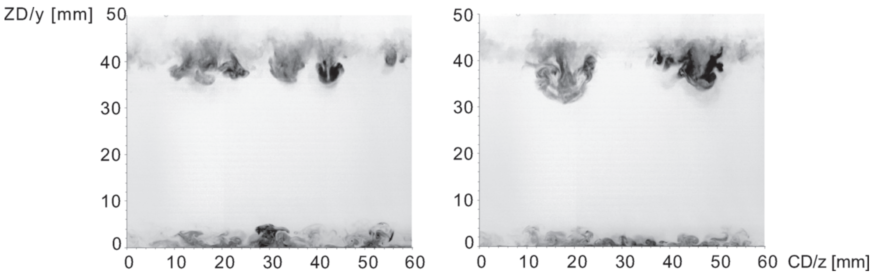

Figure 11 Two frames from the flow visualizations just under the step in the CD-ZD-plane.

visible in both frames. One has to be careful on making conclusions from the boundary layer structures, since the dye as a passive scalar tends to depict the history of the flow rather than the actual vorticity. The dye was injected in the upstream to a turbulent boundary layer and what is observed at x=0mm may result from the vorticity prior to the onset of relaminarisation. Partly relaminarized boundary layer beneath the step does not have the vorticity to transport the dye anymore.

One of the important questions that were originally motivating the present study was, what kind of interaction there is between the slice bar and bottom wall boundary layer. The principal mode of interaction is naturally the acceleration due to the sudden contraction, which was explored in terms of the time-mean turbulence quantities above. In addition to the mean flow pattern, other modes of interaction are conceivable. The appearance of strong vortex pair close to the step might create a disturbance, which would affect the flow on the bottom wall. To study if this kind of mechanism could be found in the present case, data in the *z*-*y*–plane was analyzed carefully. The flow visualizations or PIV-data do not indicate any direct momentum

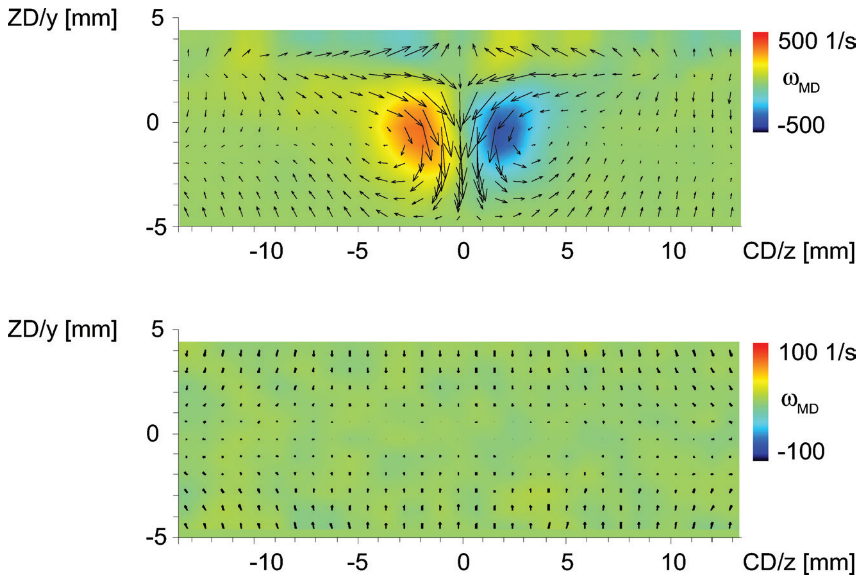

Figure 12 Conditionally averaged flow patterns related to a strong negative velocity under the FFS. The upper image corresponds to the average flow pattern just beneath the step and the lower one the flow pattern in the vicinity of the bottom wall.

transfer between the layers. Even though the flow structures from the step shear layer occasionally extend to the half way between the step and bottom wall, actual pairing of the vortices in these layers cannot be observed. This may happen later in the downstream, which is out of the measurement region in the present study. Another strategy is developed to look for possible interaction around the position x=0mm. Conditional averaging is utilized to reveal if the occurrence of strong vortex pair in the shear layer induces something typical on the opposite wall. In each instantaneous field the magnitude of wall-normal velocity component was threshold along a spanwise line just under the step. Strong negative values signify down wash of fluid towards the bottom wall, which typically occurs due to streamwise vortex pairs. Using strong negative wall-normal velocity as the condition for averaging, a mean flow pattern presented on top of the Figure 12 is obtained. This flow field is established by cropping and storing a window with a size of $25\times10mm^2$ centered to the location of the maximum down wash and averaging over the collected samples. Every time a sample is cropped, the flow pattern on the opposite wall is stored too. This way the conditional average- and rms-fields for the boundary layer can be established. Conditional average of the boundary layer flow pattern is presented also in the Figure 12. This analysis does not bring forward any secondary flow structure or even increased turbulence energy compared to randomly sampled locations. To further verify this result, some sequences, in which streamwise vortex pair remains at a constant location over several frames are analyzed by visually inspecting the vorticity fields close to the bottom wall. The results from this study do not either reveal any characteristic structure related to long streamwise vortex pairs on the opposite wall.

The flow around the slice bar has also been studied numerically. Figure 13

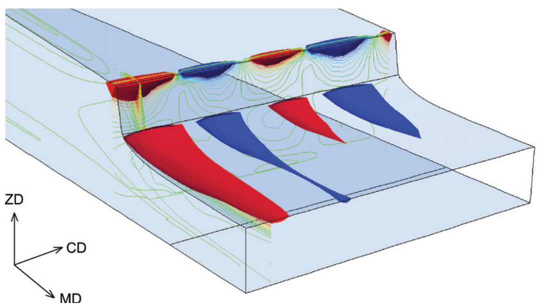

Figure 13 Numerical simulation of the flow around the slice bar.

show a result from a CFD simulation in which the ability of slice bar to intensify upstream disturbancies was evaluated. This figure shows that the presence of slice bar greatly increases the magnitude of initially weak cross-flows (red and blue colors correspond to positive and negative U_{CD}-component respectively). This figure is attached here to show that also simulation can be used to understand the significance of these phenomena. However, more work and validation with experimental results are needed to reliable predict the instabilities discussed here.

4 DISTURBANCES GENERATED BY THE VANES

The disturbance generated by the vanes manifests itself predominantly as a stable array of high-velocity streaks in the wake of the vane. This periodic secondary flow structure inherits in paper as highly-organized streakiness. Sometimes also the periodic shedding of CD aligned tip vortices may leave their imprint the paper [3], but all this is actually related to the same phenomenon. Figure 14a shows a mean velocity field measured in the MD-CD –plane just after the vane tip at ZD=0 (see Figure 3). The flow direction (MD) is from bottom to top. Superimposed on the streamwise accelerating base flow one can observe streamwise streaks of relatively higher velocity with CD spacing in the order of 10mm. The amplitude of the streaks in the present example is about 10% of the mean velocity. Figure 14b displays a paper sample, in which fibers in the middle layer are dyed blue and their penetration to the sheet surface is studied. Again the CD is on the horizontal axis. The color of the

a)

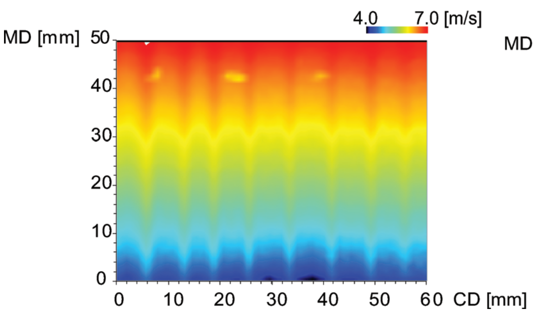

b)

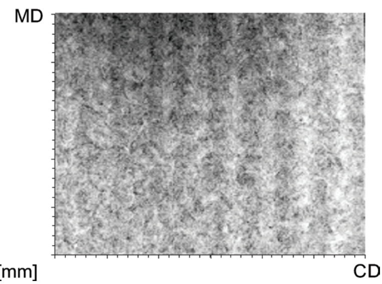

Figure 14 Mean-velocity field in the MD-CD-plane just behind the vane tip (a), and stable MD-streakiness in a paper sample (b).

paper surface clearly shows streakiness, which does not meander or change in scale in MD. Transparently these two figures show a striking similarity in appearance. These two results are not from the same case, since PIV experiments are not possible in the real process. However, comparison between pilot-machine paper samples and laboratory-scale water experiments show a very good correlation in terms of the conditions of streak appearance and their CD-spacing.

An extensive experimental campaign has been carried out to determine the actual fluid dynamical mechanism creating the streaks in the mean flow field and subsequently in paper. The most important results and observations of this body of research will be presented in the following. First, a short introduction to the physics of the flow around the vane tip is presented.

4.1 Vortex shedding and resulting fluid-structure interaction

As the flow passes the vane tip, the conditions will change from a wall-bounded shear-flow (boundary layer) into a free-shear layer (wake). In other words, the flow separates from the body, which comprises strong and complex instability mechanisms. The flow separation at the tip of a vane generates a wake dominated by periodic shedding of spanwise (CD) vortices. This is the famous Kármán vortex street. Despite the very simple configuration, the shedding of vortices displays extremely complex fluid dynamics. The instability mechanisms inducing vortex shedding are principally inviscid in nature and controlled by mean velocity profiles. Therefore, very similar flow structures are observed behind different kind of trailing edge (tip) designs. It is important to note that vortex shedding is *not* turbulence in essence, but periodic shedding of large-scale vortices takes place also at very low Reynolds numbers in laminar flows. Turbulence comes into the picture as three-dimensionality, which actually introduces irregularity and random fluctuations to the well-ordered vortex shedding. Figure 15 displays Kármán vortices shedding from the tip of a vane. This wake is turbulent, which is the case always in the headbox applications. Contours in the background represent spanwise vorticity and the vectors the in-plane velocity components (u_{MD} and u_{ZD}) with a mean streamwise convection velocity subtracted. Thus, the vectors in the middle of the wake appear to point upstream, even if the real velocity is to the downstream direction. Turbulence in the wake manifests itself as small-scale streamwise vortices and large-scale vortex dislocations.

Fluctuating pressure field related to the vortex shedding generates unsteady force acting on the vane tip. Depending on the vane material and the intensity of vortex shedding, the vane may be able to respond to the force, i.e. it may be able to move or deflect. If this is the case, one ends up with a fluid-structure

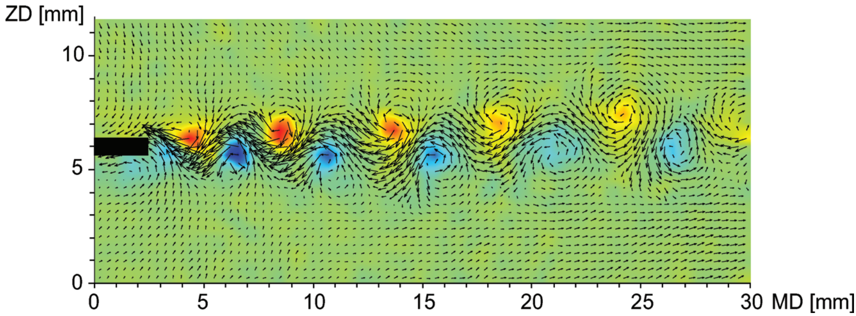

Figure 15 Kármán vortices in the wake of a vane. The vane tip is on the left and flow is from left to right.

interaction (FSI), or more specifically vortex-induced vibration (VIV). The vane is typically able to responds in ZD, by moving or deflecting up and down at the same frequency as the vortices are shedding. This movement introduces a mechanism of spanwise forcing to the flow, so that the coherence of spanwise vortices increases. This increase, in turn, synchronizes the pressure forces along a great length over the span, which means even higher amplitude of oscillation. Very small amplitude, i.e. only a few percent of the tip thickness, is enough to cause significant increase in the spanwise correlation length. These highly organized vortices are not turbulence according to the definiton and besides the fluid mechanical parameters and vane dimensions, their magnitude also depends on the mechanical properties of the vane, i.e. mass, stiffness and structural damping.

A vast amount of literature concerning wakes and vortex shedding after bluff bodies can be found. Very good reviews on this subject can be found in references [23, 24, 25]. Also the subject of VIV is widely studied. For excellent reviews on this topic the reader is referred to [26, 27].

4.2 Observations in the wake of a vane

In this section we are trying to provide the reader with the fundamental observations of wakes behind vanes and parameters critical to the appearance of the streaks. Two examples of mean-flow fields measured in the MD-CD plane at ZD=0mm just after the tip of a vane are presented in Figure 16. Here, an in the following figures, the speed label denotes the speed of the slice jet in the given setup. In Figure 16a, one can see a smooth mean-velocity profile in CD. This is not the case in Figure 16b, where a distinct array of

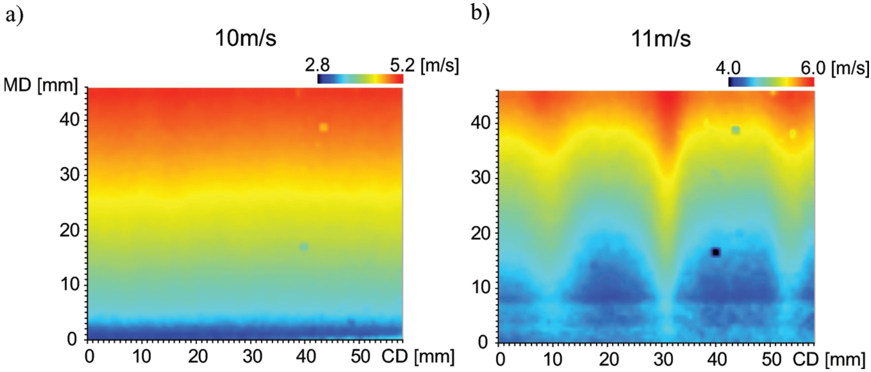

Figure 16 Examples of even and streaky mean-velocity fields after the vane in the MD-CD-plane.

streamwise streaks is observed. The streaks are actually spatially concentrated regions of relatively higher velocity. In most cases this secondary flow pattern is not mixed prior to the slice jet, but preserves its scale and coherence down to the jet. The difference between these two cases is only in the flow velocity. The streaks are established above a threshold velocity, which for this particular vane is about 5.5m/s (measured at the vane tip, outside the wake). Thus, this pair of images demonstrates that the appearance of streaks is a function of flow velocity. The streak spacing decreases as the flow velocity is increased. This is clearly observed in Figure 17. The streak spacing is also a function of the tip thickness, which is evident from Figure 18. Here, three different tip thicknesses are measured at exactly the same flow conditions. Thicker tip clearly results larger streak spacing. Furthermore, the thicker the tip is, the larger threshold speed is needed to create the streaks. The amplitude (magnitude) of the streaks with thick tips is large compared to those generated by thin tips. Depending on the tip thickness and the flow velocity, the streak spacing varies between 5mm and 40mm. Also the material of the vane has an important contribution to the streak generation. This is an obvious consequence of the fact that streaks are related to the vibration of the vane. Figure 19 shows three mean-velocity fields again in the same position. Now the only difference between the data sets is the material of the vane. The flow speed and the vane design including the tip thickness, which is 0.4mm, are the same in all cases. Aluminum produces larger streak spacing than polycarbonate and stainless steel does not produce any clear streakiness at this speed. Heavier and stiffer vanes are more resistant to vibrations generating the

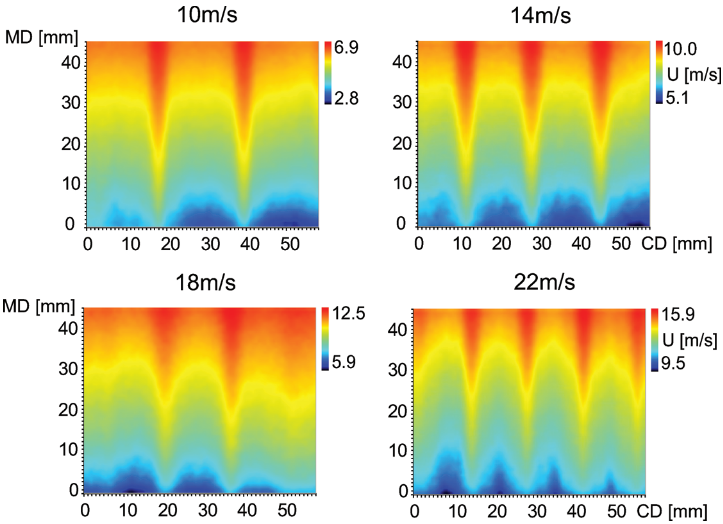

Figure 17 The effect of flow rate to the streak spacing.

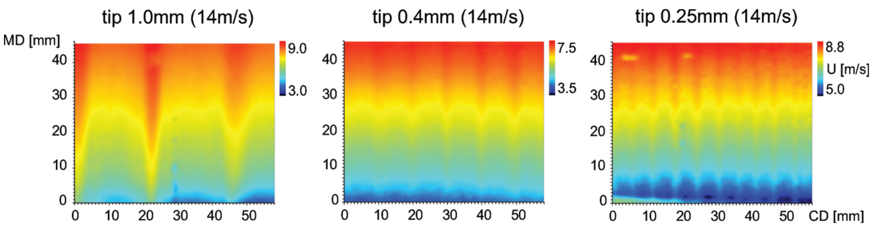

Figure 18 The effect of tip thickness to the streak spacing.

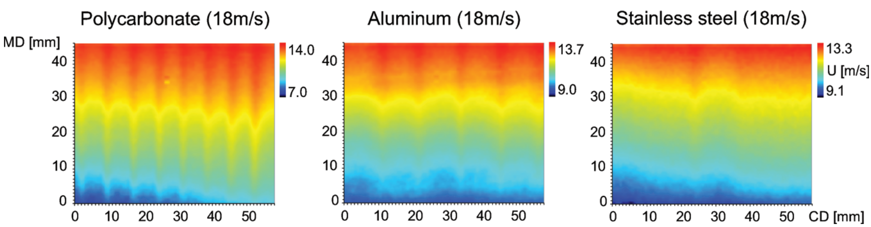

Figure 19 The effect of vane material to the streak spacing.

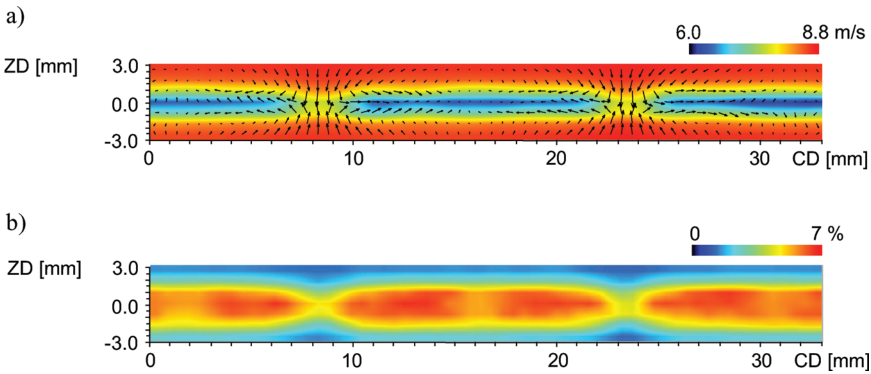

Figure 20 Mean-velocity and turbulence intensity fields in the CD-ZD –plane 10mm after the vane tip.

streaks. Note that a 0.4mm thick tip produces significantly narrower streak spacing and weaker streaks than 1.0mm thick tip at the same flow rate (cf. to Figure 17) and that the streak spacing with the 0.25mm polycarbonate tip at 14m/s is very close to that of the 0.4mm tip at 18 m/s (cf. to Figure 18).

Next the flow physics behind the streaks will be explained. Figure 20a shows a reconstruction of the mean-flow pattern in the CD-ZD –plane, about 10mm after the vane tip. This plane cannot be directly measured, but the mean-flow pattern can be constructed from the data measured in the other planes. What appears as an array of streamwise streaks in the MD-CD-plane, is actually a cellular pattern from this view, i.e. in the CD-ZD-plane. A regular sequence of low-speed cells divided by narrow high-speed regions is established along the tip in CD. Figure 20b presents the turbulence intensity field corresponding to the mean-velocity field in Figure 20a. From here it is apparent that high turbulence energy is related to the low-speed regions, or cells. Velocity fluctuations are very low within the high-speed streaks. Most of the energy contributing to the velocity fluctuations is due to the vortex shedding, as will be demonstrated next. Again, strictly speaking, high level of turbulence kinetic energy is not really related to turbulence, but periodic velocity fluctuations due to the vortex shedding, which is a result of FSI. Conventional analysis of the velocity signal is unable to distinguish between random and deterministic fluctuations.

To elucidate the point made above about the concentration of vortex shedding to the low-speed cells, two instantaneous velocity fluctuation fields (left) with corresponding average field (right) are presented in Figure 21. Contours

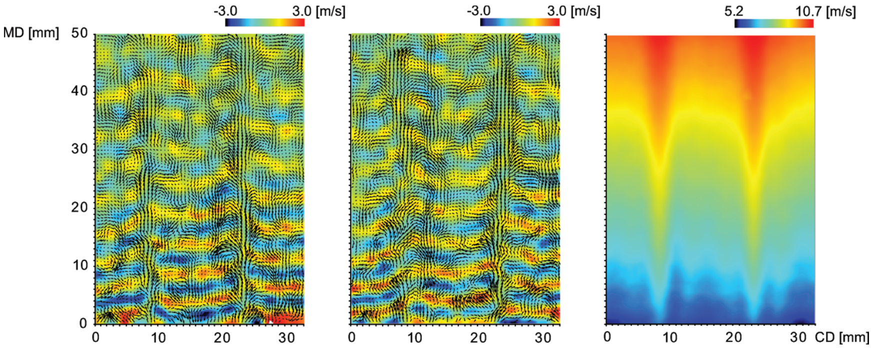

Figure 21 Two examples of instantaneous velocity fluctuation fields in the MD-CD – plane just after the vane tip and the corresponding mean-velocity field.

in the background of the instantaneous fields correspond to the u'$_{ZD}$-component and the vectors to the u′$_{MD}$- and u′$_{CD}$-components, respectively. Periodic vortex shedding patterns in the contours of u'$_{ZD}$ are striking in both images. Alternating rows of blue and red correspond to positive and negative values of u'$_{ZD}$, which are created by counter rotating Kármán vortices (see the vectors in Figure 15). The vortex tubes, i.e. CD-aligned worm kind of contours of u'$_{ZD}$, show high spanwise coherence over the entire cell, i.e. between the high-speed streaks in the average field. The energy of vortex shedding is low within the high-speed streaks. To further confirm the spanwise uneven distribution of vortex shedding, the instantaneous velocity fields measured MD-CD-plane are analyzed by computation of the streamwise Power Spectral Density (PSD) estimate as a function of the CD position. The results are shown in Figure 22, where the spectrum of u'$_{ZD}$-component is presented. The CD position is on the abscissa and the wavelength on the ordinate. Color indicates the energy of vortex shedding. Cellular structure is evident also in this analysis. Spanwise variation of the turbulence energy was already observed in the turbulence intensity field, in Figure 20b. Now the spectrum shows, that the velocity fluctuations are related to a very narrow wavelength band. The dominant shedding wavelength around 5mm is clearly visible and fairly constant across the span of the measurement window, even though the energy varies considerably. To conclude the results presented so far in one sentence: The streaks in the mean-velocity field are created by spanwise clustered variation of vortex shedding energy.

The reason for this cellular shedding lies in the vibration of the vane, which will be demonstrated next. In Figure 23, the spectrum of vane vibration is

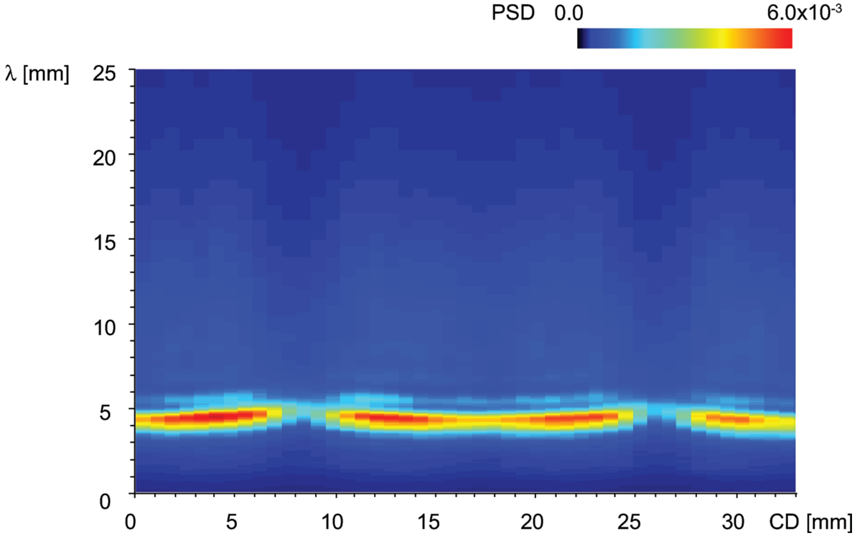

Figure 22 Streamwise spectra for u_{ZD}-component in the near wake over a short span in CD.

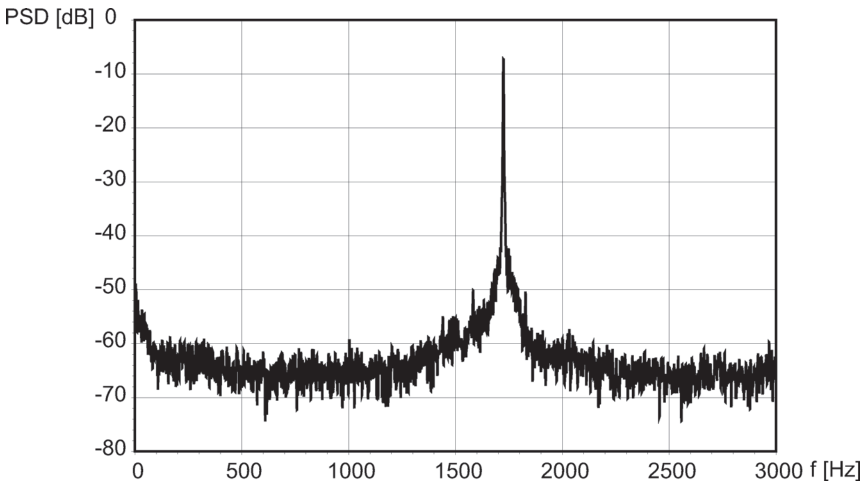

Figure 23 The spectrum of vane vibration.

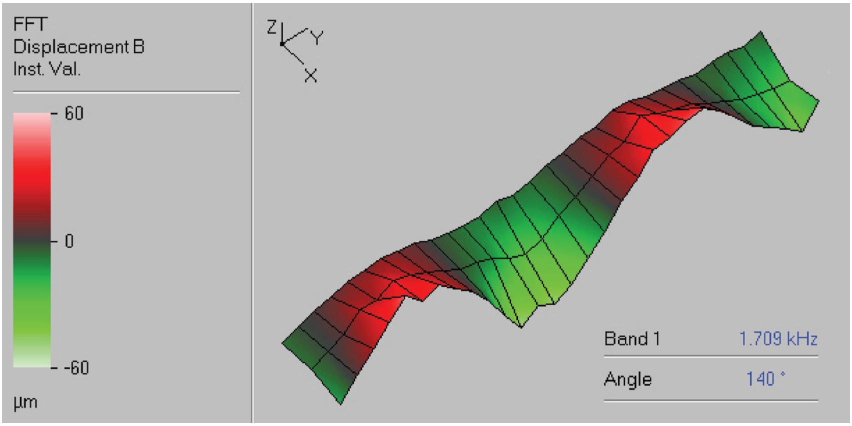

Figure 24 The vibration mode of the vane tip resulting from modal analysis (x=MD, y=CD). The color correspond to the instantaneous magnitude of deflection of the tip.

presented. This spectrum is measured as an average over the area indicated in Figure 4. The spectrum is dominated by a peak at 1709Hz. LV-system can be used for modal analysis, which yields the 2D vibration modes of the structure related to each peak in the spectrum. The result of the modal analysis for the peak at 1709Hz is presented in Figure 24. This is a snapshot from an animation, which shows the full phase-amplitude information of the vibration mode. The CD span of the measurement area is 60mm and the MD-length about 10mm. The color corresponds to the magnitude of deflection of the tip in µm. This analysis reveals that, the mode corresponding to the dominating frequency peak is a standing wave settled along the vane trailing edge. The wavelength of the standing wave corresponds to the spacing between the high-speed streaks and the frequency is that of the vortex shedding. Depending on the type of the vane and flow velocity, the amplitude of the standing wave varies from nanometers to hundred micrometers. One can also plot the variation of the vane tip vibration energy as a function of the CD-position, as presented in Figure 25 (lower profile). This plot shows again a distinct cellular pattern. For comparison, the plot also includes CD-profile of mean-velocity in the same case. The coincidence between the nodes of the standing wave and the high-speed streaks is not perfect in Figure 25, since these two quantities cannot be measured simultaneously and some scatter in the data is always expected for such a sensitive phenomenon). However, it is clear that the high-speed streaks do coincide with the nodes of the standing wave. Having seen all this, the following picture emerges:

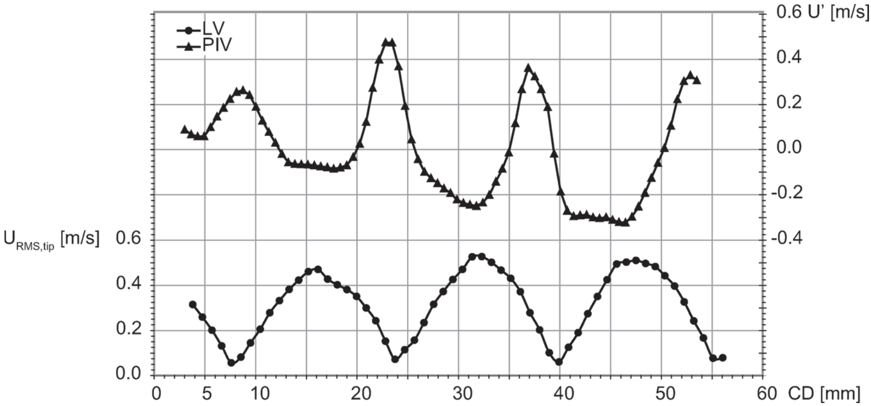

Figure 25 Comparison between the CD-profiles of vibration energy (LV) and normalized U_{MD} in the near wake (PIV).

> *Vortex shedding, which is an inherent part of a bluff body wake, forces the vane to vibrate at the vortex shedding frequency. (The resulting frequency may shift a little bit from the natural shedding frequency due to the synchronization). This evokes a complex fluid-structure interaction. The vane responds to forcing in a characteristic vibration mode, which in some cases takes the form of a standing wave along the trailing edge. As a result of this vibration mode, the amplitude of vibration varies along the span in such a way, that the amplitude is very close to zero in the nodes of the standing wave and in the anti-nodes reaches a level of about 20–100μm in those cases, in which the streaks in the mean-velocity field are observed. Thus, the resulting vibration mode enhances vortex shedding in the anti-node locations and locks the vortex shedding into distinct cells between the nodes of the standing wave. The "streaks" are established at the nodes, in which the wake has minimum width and velocity fluctuation energy.*

At this point it must be emphasized that almost all the vanes do shed vortices, but they do not create problems, since the frequency or magnitude of the vortices is not susceptible to induce FSI under that particular set of parameters (velocity range, tip design, and vane material). Also all the vanes do vibrate, in a standing wave mode or some other (random) mode, but the amplitude is not enough to lock-in the vortex shedding to create the streaks. Experimental evidence shows that an amplitude of 20–30μm is needed to lock-in the vortex shedding to create streaks.

4.3 Discussion

Although the results above present a quite coherent picture of the phenomena, several details of the physical mechanism remain unclear. The vortex shedding from the tip has clearly a governing role on the onset of the vibration mode. The vibration mode and thus the streaks do not appear if the vortex shedding does not occur. However, it is unclear if the vortex shedding is the only source of energy feeding the vibration mode. The supply of additional energy may occur through the mechanical vibration of the hinge or as a boundary layer excitation due to the pressure forces along the vane surfaces. It can be speculated that random and low-frequency vibrations feed the energy to the high-frequency mode excited by the highly periodic and strong forcing due to the vortex shedding at the tip. If this is the case, only the frequency of vibration may be determined by the tip design and the energy of vibration would be merely fed by the flow and low-frequency structural vibrations.

Then, the relationship between the primary vibration frequency and tip thickness remains vague. If only the fluid mechanics would determine the vortex shedding frequency, there would be no difference between materials in respect to the vibration frequency. But since we are dealing with a FSI, also the natural frequencies of the structure, damping and so on, enter the process. There are slightly contradictory results on the effect of the material on vortex shedding frequency. For thick tips (1 mm) no difference in the vortex shedding frequency has been observed between stainless steel, aluminum and polycarbonate. In contrast, for thin tips (0.4 mm), there are clear differences between the frequencies for various materials. It may happen that different physical mechanism is controlling the frequency selection in these cases.

Also the exact relationship between the vibration frequency and the streak spacing, i.e. the wavelength of the standing wave, is unclear. Typically the ratio between the CD-spacing of the streaks and the wavelength of the vortex shedding is in the order of 4 to 5. Here, the natural frequencies and modal response of the vane are obviously important.

5 CONCLUSIONS

This paper presents two sources of flow instability in the headbox nozzle. Both of these instabilities may result in disturbances with considerable magnitude and thus inherit in paper. Due to the increasing demands set on paper and board quality, the possible effects of this kind of disturbances must be taken into account while designing the headbox hydraulics. To put another way, the traditional optimization of turbulence and residence times is not the only requirement for high quality headbox hydraulics, but also effective control of flow instabilities developing separately from turbulence needs to be addressed. In this study, academic experimental setups are used to isolate the fundamental fluid mechanics to understand the origin of these phenomena.

The first instability is related to the highly asymmetrical the geometry of the headbox nozzle exit, which creates a sudden acceleration and streamline curvature. The results presented in this paper show that the primary mode of interaction between the slice bar and the boundary layer on the bottom wall, results from the mean acceleration field. Strong favourable pressure gradient tends to relaminarize turbulent boundary layer on the lower lip. This trend is obvious in the present case, even if complete relaminarisation cannot be observed. However, remarkable alterations in the structure of turbulence inside the boundary layer are observed. Compared to the boundary layer turbulence, the structures evolving in the slice bar shear layer are an order of magnitude stronger. In essence, the slice bar model utilized in the present experiment creates strong streamwise vortices. The length scale of these vortices is estimated and it is shown to be an order of magnitude larger than the slice bar stick-out length. Direct impact of these structures to the relaminarizing boundary layer is studied by flow visualization and conditional averaging of the PIV-data. However, no indication of direct interaction between these vorticity layers is observed.

The second instability is related to the tip of the vane. Recent experimental work has revealed the reason for the streakiness observed in the CD-profiles of the mean-velocity created by some vanes at certain speeds. The streaks results from a fluid-structure interaction, in which the flow excites the vane to respond in a characteristic vibration mode. In some cases, the vibration mode takes the form of a standing wave along the tip of the vane. The standing wave results in unevenly distributed vortex shedding energy in CD. In the flow field, this appears as a cellular vortex shedding pattern. Secondary flows related to the cellular shedding leave the imprint in the mean velocity field as high-speed streaks, which are actually located in the CD-positions, where the vortex shedding energy reduces to minimum. These are the locations of the nodes of the standing wave. PIV (for the flow) and LV (for the vibration) measurements are used to show the effect of the vane tip design, the flow rate and the vane material on the streaking problem.

Both slice elements scrutinized in this paper, have a clear functionality in papermaking, but under certain circumstances they are susceptible to flow instabilities that may influence the sheet quality. For example, the FSI of the vanes is highly dependent on the Reynolds number, i.e. the flow rate. Thus, problems may be encountered only at certain speeds and concepts proven in the certain running conditions may show unwanted behavior at the higher speeds of future papermaking machines.

ACKNOWLEDGEMENTS

The authors are very grateful to the following people involved in these research projects: Pentti Saarenrinne (Tampere University of Technology, Tampere, Finland), Petri Jetsu, Janne Lappi and Panu Ärölä (Metso Paper Inc., Jyväskylä, Finland), Janne Poranen and Hannu Sekki (VTT Process, Jyväskylä, Finland), Tim Wei and Tsun-Ya Hsu (Rutgers; The State University of New Jersey, USA), and Piroz Zamankhan (Lappeenranta University of Technology, Lappeenranta, Finland). Also the grant from Academy of Finland (grant no. 104835) is gratefully acknowledged.

REFERENCES

1. M.H. Odell and P. Pakarinen. The compleat Fibre Orientation Control – and Drivers Effects on Paper Propertied, In the Proc. of XII Valmet Paper Technology Days, 2000.
2. H. Karema, J. Salmela, M. Tukiainen and H. Lepomäki. Prediction of paper formation by fluidization and reflocculation experiments. Proceedings of the 12th FRC Symposium, September 19th–21st 2001, Oxford, England.
3. P. Jetsu, M. Kellomäki, H. Karema, J. Salmela, T. Lappalainen and M. Piirto. Coherent structures of suspension flow and their inheritance in paper. Proceedings of the 12th FRC Symposium, September 19th–21st 2001, Oxford, England.
4. M.D. Lloyd and B. Norman. Use of stepped vanes to alter headbox turbulence levels during stratified forming of woodfree paper. Appita Journal, 52:2, pp. 98–104, 1999.
5. H. Lepomäki, J. Huovila and H. Karema. Control of paper properties by headbox fluid dynamics. Presented in the 96th Zellcheming Annual Meeting, 25th–28th, June, 2001, Baden-Baden. Germany.
6. D. Söderberg. Hydrodynamics of Plane Liquid Jets Aimed at Applications in Paper Manufacturing, Doctoral Thesis, Royal Institute of Technology, Department of Mechanics, FaxénLaboratoriet, Stockholm, Sweden, 1999.
7. T.-Y. Hsu. Hydrodynamics of Paper Making: Streamwise Vortices Generated in Upstream of a 2-D Jet Nozzle, Doctoral Thesis, Rutgers; The State University of New Jersey, USA, 2002.
8. H. Eloranta, T.-Y. Hsu, T. Wei and P. Saarenrinne. A PIV study on the interaction between a forward-facing step and turbulent boundary layer. In the Prof of Application of Laser techniques to Fluid Mechanics, July 10th–13th, 2002, Lisbon, Portugal.

9. H. Eloranta, T.-Y. Hsu, T. Wei and P. Saarenrinne. On the interaction between a forward-facing step and turbulent boundary layer. In the Proc of. Third International Symposium on Turbulence and Shear Flow Phenomena, Sendai, Japan, June 25–27, 2003.
10. M. Steen. Turbulence and flocculation in fibre suspensions, Doctoral dissertation, Division of Thermodynamics, University of Trondheim, Norway, 86p., 1990.
11. M. Raffel, C. Willert and J. Kompenhans. Particle Image Velocimetry – A Practical Guide, Springer, 1998.
12. D.J. Ewins. Modal Testing – theory, practice and application. Research Studies Press Ltd, 2000.
13. H. Eloranta, T. Pärssinen and P. Saarenrinne. Fluid structure interaction in the wake of a splitter plate. Part 1 – Analysis of cellular vortex shedding with PIV. Submitted to Experiments in Fluids (in review).
14. H. Eloranta, T. Pärssinen and P. Saarenrinne. Fluid structure interaction in the wake of a splitter plate. Part 2 – Analysis of plate vibration with Digital Imaging and Laser Vibrometer. Submitted to Experiments in Fluids (in review).
15. H. Eloranta and P. Saarenrinne. The structure of turbulence in the near-wall area of a channel flow. Proceedings of the 12th FRC Symposium, September 19th–21st 2001, Oxford, England.
16. R.F. Blackwelder and L.S.G. Kovasznay. Large-scale motion of a turbulent boundary layer during relaminarization, J. Fluid Mech., 53. pp. 61–83, 1972.
17. M.P. Escudier, A. Abdel-Hameed, M.W. Johnson and C.J. Sutcliffe. Laminarisation and re-transition of a turbulent boundary layer subjected to favourable pressure gradient. Exp. in Fluids, 25, pp. 491–502, 1998.
18. R. Narasimha and K.R. Screenivansan. Relaminarization of fluid flows. Advances in applied mechanics, vol 19, pp. 221–309, 1979.
19. U. Piomelli, E. Balaras and A. Pascarelli. Turbulent structures in accelerating boundary layers, Journal of Turbulence, http://jot.iop.org/, 1/2000.
20. K.R. Screenivasan. Laminarescent, relaminarizing and retransitional flows. Acta Mechanica, 44, pp. 1–48, 1982.
21. P.R. Spalart. Numerical study of sink-flow boundary layers, J. Fluid Mech., vol. 172, pp. 307–328, 1986.
22. M. Parsheh. Flows in contractions with application to headboxes, Doctoral thesis, Royal Institute of Technology, Department of Mechanics, FaxénLaboratoriet, Stockholm, Sweden, 2001.
23. P. Huerre and P.A. Monkewitz. Local and global instabilities in spatially developing flows, Annu. Rev. Fluid Mech., 22, pp. 473–537, 1990.
24. H. Oertel. Wake behind blunt bodies, Annu. Rev. Fluid Mech., 22, pp. 539–534, 1990.
25. C.H.K. Williamson. Vortex dynamics in the cylinder wake, Annu. Rev. Fluid Mech., 28, pp. 477–539, 1996.
26. P.W. Bearman. Vortex shedding from oscillating bluff bodies, Annu. Rev. Fluid Mech., 16, pp. 195–222, 1984.
27. C.H.K. Williamson and R. Govardhan. Vortex-Induced Vibrations, Annu. Rev. Fluid Mech., 36, pp. 413–455, 2004.

Transcription of Discussion

FLUID MECHANICS OF THE HEADBOX NOZZLE: COHERENT FLOW STRUCTURES, INSTABILITIES AND DISTURBANCES CLOSE TO THE NOZZLE EXIT

Hannu Eloranta,[1] *Hannu Lepomäki*[2] *and Tero Pärssinen*[1]

[1]Institute of Energy and Process Engineering, Tampere University of Technology, P.O.Box 589, FIN-33101 Tampere, Finland
[2]Metso Paper Inc., P.O. Box 587, FIN-40101 Jyväskylä, Finland

James Watkins Proctor and Gamble

It sounds like you are concluding that we should be making our vanes from stainless steels?

Hannu Eloranta

It is not that simple because they may create some other problems than the streamwise streaks. Stainless steel is not the best material to use; it is very heavy, it is very stiff. Heavy materials are good, but then there are lot of other things to consider so it is not that simple unfortunately.

Ari Kiviranta

Vanes have also been used to eliminate streakiness but now you are able to show that actually they also create some streakiness. What do you say about that?

Discussion

Hannu Eloranta

We must consider the source of streakiness they are aimed at. It seems that there are several sources of streaks. The shear flow itself is a source of unstable streakiness. This stable streakiness is only related to vanes, but then there is also streakiness that comes from the turbulence generator. That is something we can probably eliminate with the vanes. So for some conditions, the vanes work well, but then you can find situations where you end up with new problems.

Ari Kiviranta

Are there any other techniques to eliminate or at least to dampen the vibration of the vane tip other than just changing the material?

Hannu Eloranta

There is a combination of several things: the material properties, the design itself, the length. It really depends on how long the vanes are. What is their thickness? I do not know the right answer because it seems that more work is needed to understand what is really happening and which parameters are involved.

Ari Kiviranta

I have one more question about the slicebar. The slicebar is usually or traditionally used in a headbox because you need it for profiling. Now in the last 10 years there are more and more dilution controlled headboxes and dilution profiling. Do you still need the slicebar if it is causing problems, can you simply take it out?

Hannu Eloranta

I am not really an expert in papermaking, but it seems that fibre orientation and some other things can be controlled with the sudden acceleration at the exit. We have to consider how we can still do those things if we replace the slicebar with something else. The slicebar brings a lot of good things, but then there are some bad things that we should consider too. Just taking it out, I guess, will not be a solution.

Hannu Lepomäki Metso Paper Inc

I have a short comment on the previous question. Because of these instabilities, behind the slicebar, of course the obvious comment is that we should take it off. However, we still need the slicebar to create at least a small contraction of the slice jet. We need that in order to impinge the jet very accurately inside the wire cap. So I think the right answer is that we need to minimize the "stick-out" of the slicebar instead of taking it totally off.